RSC Advances

ROYAL SOCIETY OF CHEMISTRY

www.rsc.org/advances

RSC advances

ARTICLE

Layered manganese oxides for formaldehyde-oxidation at room temperature: the effect of interlayer cations

Received 00th January 20xx,

Accepted 00th January 20xx

DOI: 10.1039/x0xx00000x

www.rsc.org/

Jinlong Wang,[a,b] Dandan Li,[a,b] Peilin Li,[a,b] Pengyi Zhang,[*a,b] Quanlong Xu,[c] Jiaguo Yu[*c]

A series of K-, Mg-, Ca-, and Fe-containing birnessites were prepared by a facile comproportionation reactions of Mn^{2+} and MnO_4^- in the presence of different metal cations. As-synthesized birnessite samples were characterized by FESEM, XRD, TG and XPS. The catalytic activity toward decomposition of HCHO was evaluated under ambient temperature. Fe-birnessite showed the highest HCHO oxidation activity due to its highest content of surface hydroxyl groups. However, the CO_2 generation by Fe-Birnessite was relatively low due to the accumulation of formate species without further oxidation. The influence of different interlayer cations on the activity of birnessite was studied by H_2-TPR, O_2-TPD, and HCHO In-situ DRIFTS. The result indicates that K^+ leads to a considerable enhancement of surface oxygen activity which then facilitates the regeneration of surface hydroxyl by activating H_2O, therefore K-birnessite showed the highest CO_2 generation performance during HCHO removal at ambient temperature. HCHO of 0.5 mg/m^3 and the gas hourly space velocity (GHSV) of 1,200,000 h^{-1} (the corresponding contact time is 0.003 s) were selected to check the stability of the samples. K-Bir still showed stable activity with the removal efficiency reaching 40% under these critical test conditions. Considering the effect of introducing different metal cations, this work provide new insight to design high performance catalysts for indoor air purification.

Introduction

Formaldehyde (HCHO), one of the most prevalent indoor air pollutants, mainly comes from continuous release of residual HCHO and hydrolysis of urea-formaldehyde resin contained in wooden furniture, building materials, and household products over many years.[1,2] Long-term exposure to HCHO may cause serious health problems, thus HCHO needs to be eliminated to meet stringent regulations and improve indoor air quality. The formaldehyde in indoor environment is ubiquitous and it often exceeds the regulatory limit. In some cases, formaldehyde removal became one of the limiting factors determining the minimum ventilation rate and air cleaning requirements.[3] As a consequence, the development of a highly efficient process for its elimination is needed.

Complete catalytic oxidation of formaldehyde into CO_2 and H_2O using noble-metal-based catalysts (Pt, Pd and Au etc.) is a promising method to convert this pollutant at room temperature, making this process energetically attractive from an industrial point of view.[4-9] However, the development of a less expensive active material seems more attractive for a large-scale application. In recent years, several researchers started to investigate the HCHO oxidation catalysed by transition metal oxides, and among them manganese oxides are the most investigated material. Sekine [10] first found commercial MnO_2 can remove indoor HCHO at room temperature and proved that its final product was CO_2, harmful by-products such as HCOOH and CO were not detected. Sidheswaran et al. [3] synthesized a mixed MnO_x for long term oxidation of low-level HCHO (30 and 200 ppb). It was one of the first studies in which good reactivity can be achieved at room temperature. Recently, manganese oxides with different morphologies and structures have been synthesized and tested for HCHO oxidation. However, most of the manganese oxides just showed high temperature catalytic activities. [11-17] In our recent work, we reported δ-MnO_2 could oxidize HCHO at room temperature. We found that water had a significant impact on HCHO oxidation and could compensate the consumed hydroxyl groups to sustain the mineralization of formaldehyde at room temperature. [18]

On the other side, in recent years it has been reported that introduction of alkali metals may improve the catalytic properties of materials for oxidation of HCHO/volatile organic compounds (VOCs) due to the perturbation of electronic states of active centers.[4,5,7,20-23] For example, Zhang et al. [5,7] found addition of sodium species could induce and further stabilize negatively charged and well-dispersed Pt and Pd species, which accordingly facilitated their catalytic activity for HCHO oxidation. Nie et al. [4] also reported the HCHO oxidation reaction on Pt/TiO_2 catalyst modified by sodium ions and found that the content of surface hydroxyls were highly increased, thus room-temperature thermal catalytic activity of Pt/TiO_2 was enhanced. Furthermore, Bai et al. [21] found that the introduction of potassium ions on Ag/Co_3O_4 significantly promoted the catalytic performance for HCHO oxidation due to higher content of -OH species as well as more abundant Ag active facets. Hou et al. [22]

[a] State Key Joint Laboratory of Environment Simulation and Pollution Control, School of Environment, Tsinghua University, Beijing 100084, China.. E-mail: zpy@tsinghua.edu.cn; Fax: +86 10 62796840-602
[b] Collaborative Innovation Center for Regional Environmental Quality, China.
[c] State Key Laboratory of Advance Technology for Material Synthesis and Processing, Wuhan University of Technology, Wuhan 430070, China. E-mail: jiaguoyu@yahoo.com; Fax: +86 27 87879648

reported that the increase of potassium ions in a tunnel-structure MnO_2, i.e. OMS-2 improved the mobility of lattice oxygen, which enhanced the catalytic decomposition of benzene. Recently, Tang et al. [23] also introduced potassium ions into hollandite MnO_2 and argued that surface isolated K atoms with hybridized d-sp orbitals specifically promote oxygen activation, therefore enhance the catalytic oxidation activity of hollandite at low-temperature. To sum up, alkali metals including sodium and potassium have been explored to improve the catalytic performance of noble metal or transitional metal oxides. However, besides Na^+ and K^+, other cations like divalent and trivalent cations were not introduced, and their influence on the catalytic activity has never been explored.

Birnessite, i.e. δ-MnO_2, is a layered manganese oxides, which is built up from layers of edge-sharing MnO_6 octahedra with a certain number of water molecules and different cations (e.g. Li^+, Na^+, K^+, Ca^{2+}) between the layers.[21] Here, we synthesized a series of δ-MnO_2 with different interlayer cations such as K^+, Mg^{2+}, Ca^{2+}, and Fe^{3+} to investigate their effects on the catalytic activity of δ-MnO_2 for HCHO oxidation at room temperature.

Experimental

Catalyst preparation

Four kinds of birnessite with different interlayer cations (i.e. K^+, Mg^{2+}, Ca^{2+}, Fe^{3+}) were prepared by a redox reaction between Mn^{2+} and MnO_4^- in the presence of nitrate salt of different cations at relatively high pH as described in the literature.[24] In a typical synthesis, 14.0 g KOH was dissolved in 30 mL deionized water. 3.92 g $Mn(CH_3COO)_2{\cdot}4H_2O$ (16 mmol) and certain amount of $Me(NO_3)_n$ (6.4 mmol) were dissolved in 30 mL deionized water, and then the mixture was added dropwise into the KOH solution under vigorous stirring. Subsequently, 100 mL $KMnO_4$ (6 mmol) was added dropwise to the above suspension in 30 min under vigorous stirring. The obtained dark brown suspension was stirred for 72 h at 40 °C. Then, the precipitate was filtered off and washed with 1 M HCl and deionized water for 3 times to remove possible residue products (i.e. $Mg(OH)_2$, CaO, Fe_2O_3) before it was dried at 65 °C for 16 h. The synthetic process was illustrated in **Fig. 1**. As-synthesized birnessite samples with different interlayer cations were named as K-Bir, Mg-Bir, Ca-Bir and Fe-Bir, respectively.

Characterization

Thermal gravity analysis was used to determine the temperatures at which water molecules and other gases were released as samples were heated. The analysis was performed on a Netzsch STA 409PG Luxx® system. Samples (~20 mg) were heated from 25 °C to 900 °C at 5 °C/min with the sample held under flowing dry N_2 at 2[illegible] mL/min.Scanning electron microscopy (SEM) observations were carried out on a Hitachi 5500 field emission scanning electron micro-scope operated at 5 kV. All samples were sputtered with carb[illegible] before observation.

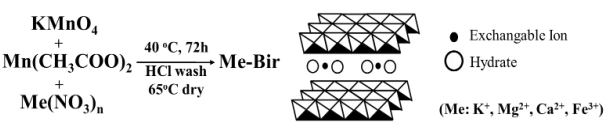

Fig. 1. Synthesis procedure of K-Bir, Mg-Bir, Ca-Bir and Fe-Bir by changing the metal nitrate.

X-ray diffraction (XRD) patterns of as-prepared samples were recorded on a Bruker D8-Advance X-ray diffractometer (Germany) using Cu K_α radiation (λ=0.1542 nm) operated at 40 kV and 40 mA. Chemical states of surface elements were investigated by X-ray photoelectron spectroscopy (XPS, PHI-5300, ESCA) at a pass energy of 50 eV, using Al K_α as an exciting X-ray source. The spectra were calibrated with respect to the C1s line of adventitious carbon at 284.8 eV. The nitrogen adsorption-desorption curves of samples were recorded by using a Micromeritics ASAP 2020 nitrogen adsorption apparatus (U.S.A.). The Brunauer-Emmett-Teller (BET) specific surface area was determined by a multipoint method using adsorption data in the relative pressure (P/P_0) range of 0.05-0.3. The single-point pore volume was obtained from the nitrogen adsorption curve at the relative pressure of 0.97. Prior to the surface area measurements, the samples were degassed in vacuum at 200 °C for 4 h.

Hydrogen temperature-programmed reduction (H_2-TPR) and oxygen temperature-programed desorption (O_2-TPD) were performed on a Chemisorb 2920 instrument (U.S.A.). As for H_2-TPR, 50 mg of sample was loaded into a quartz U-type tube. The sample was first pretreated with He (50 mL/min) at 200 °C for 1 h and cooled down to the room temperature, then the temperature was increased to 500 °C at 5 °C/min with the introduction of the reducing gas (5% H_2/Ar) at a flow rate of 60 mL/min monitored by TCD detector. For O_2-TPD, the sample was first pretreated with He (50 mL/min) at 300 °C for 30 min to remove physisorbed and interlayer H_2O as well as surface oxygen. Then it was cooled to 40 °C and flowed with O_2 gas for 30 min. After that, it was purged with He for 1 h to remove weakly adsorbed O_2. Then the temperature was increased from 40 to 500 °C at a heating rate of 10 °C/min under the flow of He gas (30 mL/min).

In-situ diffuse reflectance infrared Fourier transform spectroscopy (DRIFTS) was recorded in a Thermo Fisher 6700 instrument (U.S.A.). The sample was placed in an in-situ cell. The gaseous HCHO (80 ppm) released by paraformaldehyde powder under constant temperature were balanced by O_2 and flowed through the cell at the flow rate of 30 mL/min. O_2 and H_2O/O_2 gas were selectively used to purge the samples after 60 min of $HCHO/O_2$ reaction. All spectra were recorded by accumulating 32 scans with a resolution of 4 cm^{-1}. A background spectrum was subtracted from each spectrum.

Catalytic activity evaluation

The catalytic activity of as-prepared birnessite samples toward HCHO oxidation was evaluated through static and dynamic test respectively.

Static experiment was performed in an organic glass reactor covered with an aluminum foil on its inner wall. HCHO, CO, and CO_2 were determined with a photoacoustic IR multigas monitor (INNOVA air Tech Instruments Model 1412) online. In a typical test, 50 mg of sample was placed on the bottom of glass Petri dish with a glass slid[illegible]

cover, HCHO solution (38%) was injected into the reactor. After 1 h, the HCHO solution evaporated completely and the concentration of HCHO in the reactor stabilized. The target HCHO concentration was adjusted by the injected HCHO solution. The initial concentration of HCHO reaching adsorption/desorption equilibrium was about 200 ppm. Then the glass cover of the Petri dish was removed and the sample was exposed to HCHO pollutant. The concentrations of HCHO and CO_2 were recorded online every 2 min.

The dynamic test of as-prepared samples toward HCHO oxidation was investigated in a fix-bed quartz flow reactor (i.d. =6 mm) at room temperature. 50 mg catalyst (40−60 meshes) was used. The relative humidity was set ~48% by changing the ratio of dry air to humid air. HCHO was generated by vaporizing the paraformaldehyde, and its inlet concentration was set at ~ 0.5 mg/m^3. The total flow rate was 1 L/min with the corresponding gas hourly space velocity (GHSV) of 1,200,000 h^{-1} and the face velocity of 59.0 cm/s. The concentration of formaldehyde was measured by MBTH method.

The removal ratio of HCHO was calculated according to Equation (1):

$$\textbf{HCHO conversion}(\%) = \frac{[HCHO]_0 - [HCHO]_t}{[HCHO]_0} \times 100\% \quad (1)$$

where $[HCHO]_0$ is the inlet HCHO concentration before the exposure of the sample to HCHO, and $[HCHO]_t$ is the HCHO concentration at different time after the sample was exposed to HCHO.

Results and discussion

Structure and morphology of as-prepared samples

The phase structure of as-prepared samples was determined by XRD (**Fig. 2a**). The diffraction peaks of 2θ located ~ 12.0° (001), 24.6° (002), 36.5 ° (100) and 65.5 ° (110) can be assigned to the birnessite structure of hexagonal phase.[13, 27] The K-Bir showed sharp diffraction peaks indicating its well crystallization, while others were much weaker and wider. The interlayer distance was calculated with Bragg Diffraction equations (2):

$$2d \sin\theta = \lambda \quad (2)$$

where d is the distance of interlayer, θ is the Bragg angle, and λ is the X-ray wavelength. The interlayer distance of K-, Mg-, Ca- and Fe-type birnessite was 7.2, 7.1, 7.4 and 7.0 Å, respectively. As is well known, there are a lot of vacancy such as Mn^{3+} in the MnO_6 octahedron layer, hydrated cations between the interlayer balance the electric charge to avoid the collapse of the layers.[28, 29] The interlayer distance depends on both radius of interlayer cations and water content.[30] As can be seen from **Table 1**, potassium ion (K^+) has the largest ionic radius (1.38 Å) and Ca-Bir has the largest water content (11.5%), thus K-Bir and Ca-Bir had larger interlayer distance than Fe-Bir and Mg-Bir samples.

Table 1. Physical parameters of birnessite with different interlayer cations.

Sample	S_{BET} (m^2/g)	V_{pore} (cm^3/g)	H_2O (%)	Interlayer distance (Å)	Radius of Me^{n+}(Å)
K-Bir	96.1	0.45	7.2	7.2	1.38
Mg-Bir	128.1	0.59	9.7	7.1	0.72
Ca-Bir	207.3	0.94	11.5	7.4	1.0
Fe-Bir	158.3	0.71	6.9	7.0	0.55

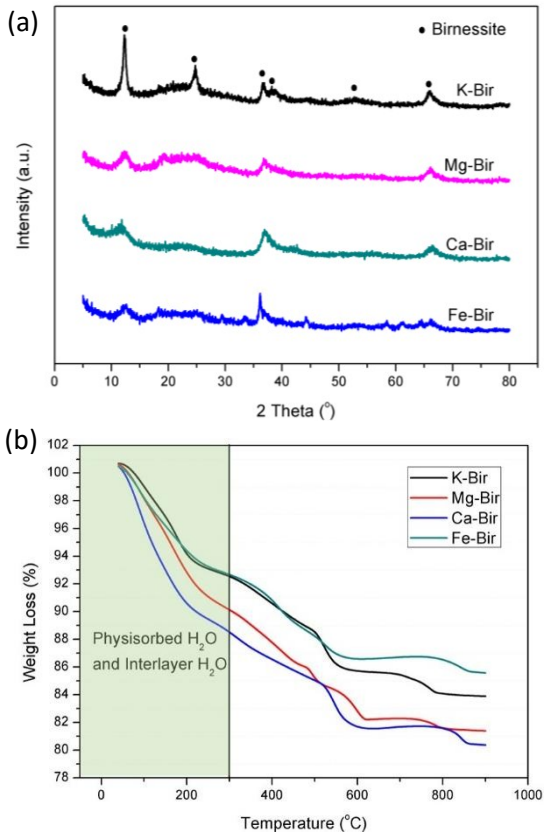

Fig. 2. (a) XRD patterns and (b) TG analysis of birnessite with different interlayer cations.

TG analysis was used to evaluate the water content contained in the different samples (**Fig. 2b**). As reported in the literature, [25] three kinds of water will be released from the layered manganese oxides with increase of temperature, which can be ascribed to weakly physisorbed water, interlayer structure water, and hydroxyl group, respectively. The former two desorbed below 300 °C were used to estimate the water content of birnessite samples. The weight loss below 300 °C for K-Bir, Mg-Bir, Ca-Bir and Fe-Bir were 7.2%, 9.7%, 11.5% and 6.9%, respectively. In the temperature range from 300 to 900 °C, the total weight was further reduced about ~20%, which can be explained by oxygen release from MnO_2 crystal lattice, resulting a stepwise reduction of manganese from Mn^{4+} via Mn^{3+} to Mn^{2+}.[26]

The specific surface area (SSA) shown in Table 1 was somewhat dependent of the water content. Ca-Bir had the highest SSA of 207.3 m^2/g) while K-Bir showed the lowest SSA (91.6 m^2/g). When the samples were degassed in vacuum at 200 °C for 4 h for SSA measurement, thus nitrogen will replace part of interlayer water and entered into the sandwich layers. While the water content of different birnessite samples depends on the inherent properties of different interlayer cations.

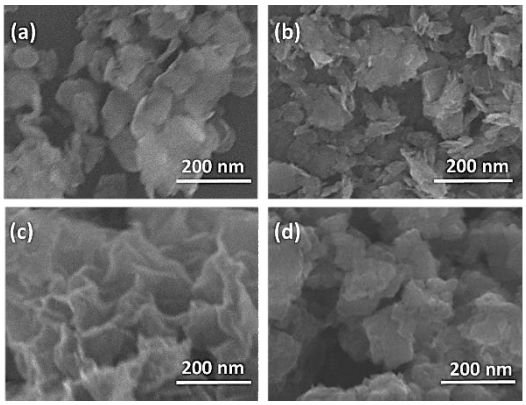

Fig. 3. FE-SEM images of birnessite with different interlayer cations (a) K-Bir (b) Mg-Bir (c) Ca-Bir (d) Fe-Bir.

The morphology of as-prepared birnessite samples were observed by SEM (**Fig. 3**). All samples consisted of 2D nanosheet, however, the sheets assembled into different morphologies, indicating the insertion of metal cations had significant effect on the morphology of birnessite. Similarly, the BET specific surface area was also much different (**Table 1**). Ca-Bir had the highest specific surface area, which is in accordance with its porous structure shown in **Fig. 3c**. The separated nanosheets was smooth and aggregated into dense particles for sample K-Bir with the lowest specific surface area.

XPS was employed to characterize the surface chemical compositions and their valence state (**Fig. 4**). K2p (the position of K2p is located around 293 eV, which is strongly influenced by C1s peak. Mg2p, Ca2p and Fe3s were observed obviously in XPS full survey spectra. Surface chemical composition and element molar ratios of different samples are summarized in **Table 2**. The ratio of Me/Mn is almost same (0.07~0.08) due to the same initial concentration of metal salt. It can be concluded that metal cations with different valence state were incorporated successfully into the birnessite layers. It has also been reported that it is possible to incorporate large amount of alkali earth ions in the birnessite even if 10-100 time high concentration of Na^+ or K^+ are present in the reaction mixture due to the very high affinity of MnO_6 layers for high-valence cations.[24] The Mn2p XPS spectrum exhibits two characteristic peaks at 642.0 and 653.5 eV, corresponding to $Mn2p_{3/2}$ and $Mn2p_{1/2}$ spin orbits. The curve-fitting analysis of the $Mn2p_{3/2}$ by XPSPEAK41 software showed the components of Mn^{3+} (641.6±0.1 eV), Mn^{4+} (642.9±0.1 eV) species.[31,32] The Mn^{3+}/Mn^{4+} ratios were calculated and summarized in **Table 2**. The Fe-Bir showed the largest Mn^{3+}/Mn^{4+} (1.38), it means that Fe-Bir had the lowest average oxidation state of Mn due to the high valence state of Fe element. The introduction of Fe may also be doped in the lattice of birnessite MnO_6 octahedral

Table 2. Surface chemical composition and element atomic ratios (per Mn) of the synthesized Me-Bir determined by XPS and ICP.

Sample	O_{-OH}/O_{latt}	Mn^{3+}/Mn^{4+}	K/Mn	Mg/Mn	Ca/Mn	Fe/Mn
K-Bir	0.26	0.42	0.21	-	-	-
Mg-Bir	0.22	0.45	0.07	0.18	-	-
Ca-Bir	0.19	0.42	0.03	-	0.17	-
Fe-Bir	0.47	1.38	0.04	-	-	0.11

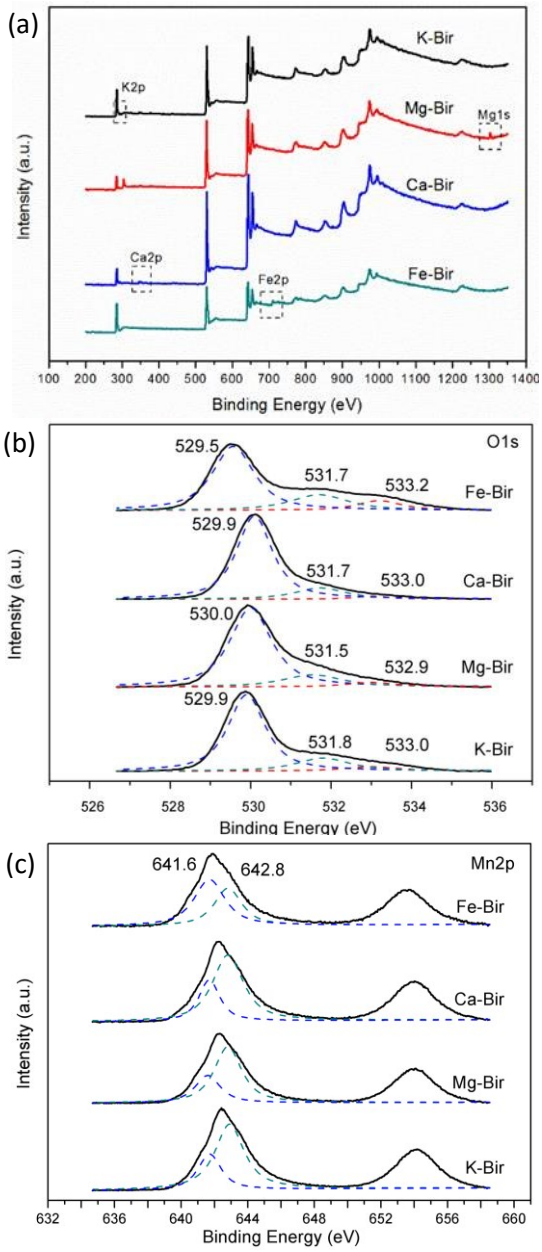

Fig. 4. XPS full survey spectra (a), high resolution Mn2p (b) and O1s (c) of different birnessite samples.

sheet due to their close ionic radius (Fe^{3+}: 0.55 Å, Mn^{4+}: 0.54 Å). As for K-Bir, it had the lowest ratio of Mn^{3+}/Mn^{4+} (0.42), which can be explained the low valence state of K^+. The O1s spectra of different birnessite samples were deconvoluted. The binding energies locat around 529.6-530.1, 531.5-532.0 and ~533 eV correspond to lattice oxygen, surface respectively.[32]. Fe-Bir showed the largest content of surface hydroxyl (O_{-OH}/O_{latt}: 1.38) compared with other ty birnessite due to large content of unsaturated oxygen caused by Mn^{3+}. Hydroxyl groups were easily formed by covalently bonding between unsaturated oxygen and he charge-compensating H[33] Besides, large content of surface hydroxyl usually result in high content of water due to hydrogen bonding between them. addition, the binding energy of lattice oxygen shifted to lower energ

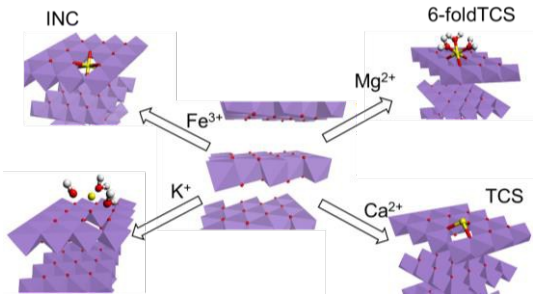

Fig. 5. Summary of reported metal cations around the Mn vacancy in birnessite. INC: incorporated inside a Mn vacancy; TCS: triple-sharing above Mn vacancy.

for Fe-Bir, while other samples did not change too much, which can be explained by the crystal distortion caused by Fe doping.

It is well known that there are metal vacancies in birnessite MnO_6 sheet, which are key sorption sites for transition metal cations through triple-corner-sharing or inner-sphere surface complexes by bonding with three unsaturated oxygen ions around a Mn(IV) vacancy.[30] As for Fe-Bir, Fe element may enter the vacancy site to become part of the sheet sheet structure, replenishing the absent Mn^{4+}. When Fe atom enters a vacancy, stress is exerted on the surrounding ions, which then is relieved by the distortion of the MnO_6 octahedral. The strong interaction between Fe-O-Mn will weaken the bond of metal-oxygen. This phenomenon was also reported in Mn doped mesoporous ferrihydrite material.[32] However, K^+ preferred to stay in the middle of interlayers due to its large ionic radius (K^+: 1.38 Å). While for Mg-Bir and Ca-Bir, cations stayed above Mn vacancies of the MnO_6 octahedra layer through triple-sharing type. The position of different metal cations inside or above the vacancy depends on their ionic radius and electron structure. The position of these cations in the birnessite is schemed in **Fig. 5**.

Activity for HCHO oxidation at room temperature

The static test of as-synthesized birnessite samples for HCHO removal at room temperature is shown in **Fig. 6**. The concentration of HCHO decreased dramatically for all the samples in the first 10 min, however, only Ca-Bir and K-Bir showed continuous HCHO removal abilities, which corresponded to the consecutive generation of CO_2. Fe-Bir showed the highest HCHO removal efficiency, reaching 80% within 60 min. However, the transformation of HCHO into CO_2 was only 16 ppm in 60 min. Though K-Bir showed somewhat lower HCHO removal efficiency (62%), its CO_2 conversion (47 ppm within 60 min) was the highest among all birnessite samples. Considering the physical adsorption of HCHO, the specific surface area of different samples were investigated. As seen from Table 1, K-Bir showed the lowest specific surface area (96.1 m^2/g) and pore volume (0.45 cm^3/g) while its CO_2 generation amount was highest compared with other samples. Furthermore, the final concentration of HCHO kept stable for Fe-Bir, while it continuously decreased for K-Bir, which implies that the intermediate such as formate species may accumulate over Fe-Bir and inhibit the sustainable oxidation of HCHO.

The activities of different samples were also tested in a flow-through reactor. Considering the concentration of formaldehyde in

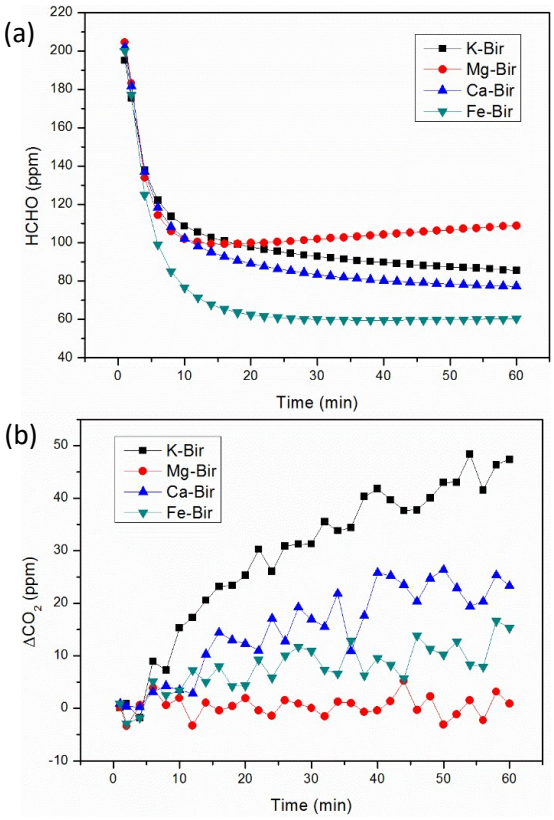

Fig. 6. (a) The concentration changes of HCHO and (b) the generation of CO_2 as a function of time over different birnessite samples HCHO removal and CO_2 conversion.

indoor environment and the short contact time required by the air cleaning system, formaldehyde of 0.5 mg/m^3 and GHSV of 1,200,000 h^{-1} were selected to investigate the activities of different samples. The corresponding face velocity was 58.9 cm/s, which is similar to that used in the literature. [3] However, the residence time (0.003 s) adopted in our experiments is much lower than that used in the literature (0.0508 s). **Fig. 7** shows the HCHO removal efficiency by different birnessite samples. The K-Bir sample showed the removal efficiency of 40% and it kept stable during 10 h testing. Fe-Bir showed

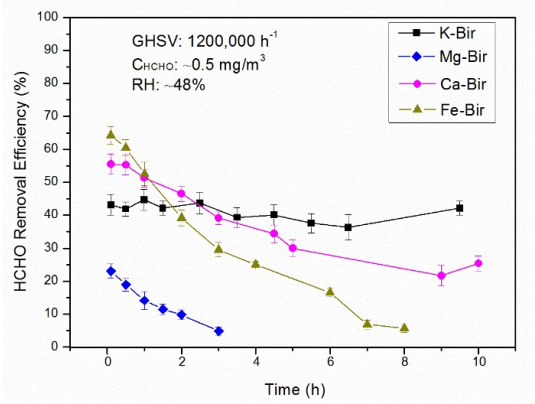

Fig. 7. The removal efficiency of HCHO as a function of time over different birnessite samples HCHO removal efficiency.

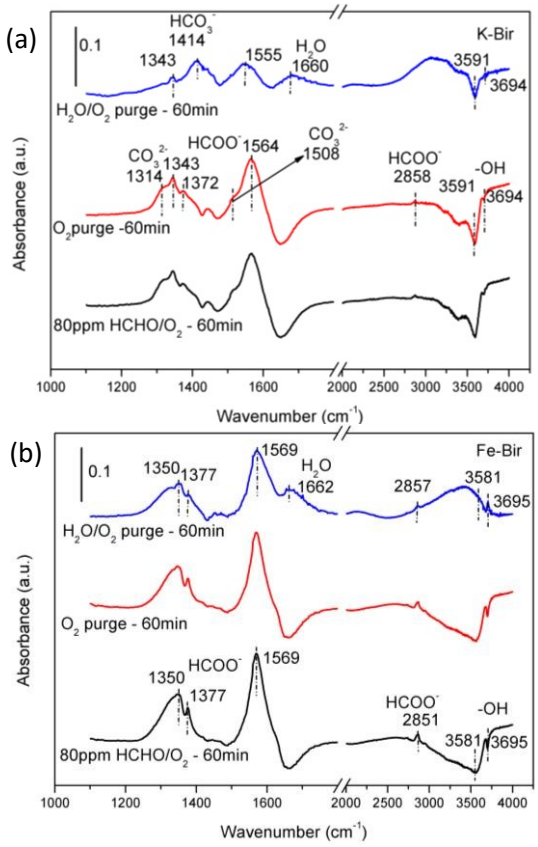

Fig. 8. In-situ DRIFTS spectra of (a) K-Bir and (b) Fe-Bir samples after a flow of 80 ppm HCHO/O_2 for 60 min followed by O_2 purging for 60 min and finally by H_2O/O_2 purging for 60 min at room temperature.

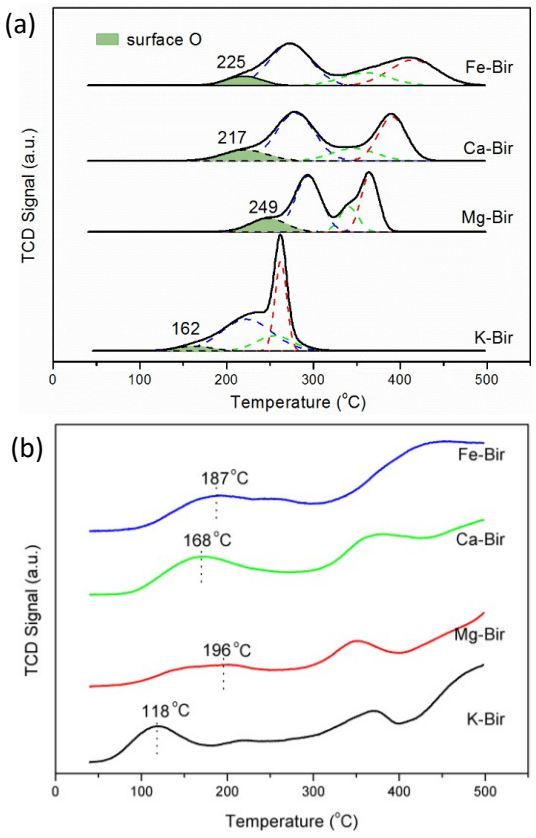

Fig. 9. H_2-TPR (a) and O_2-TPD (b) of birnessite samples with different interlayer cations. Green area is the reduction peak of surface oxygen

the highest HCHO removal efficiency at the starting stage, reaching 66.1%. However, it dropped dramatically to less than 40% in 2 h. Layered manganese oxides with other cations except K^+ also showed deactivation trend at different extent. These results indicate that the changes in the surface and bulk properties of birnessite caused by interlayer cations have significant effect on HCHO removal.

In-situ DRIFTS

In-situ DRIFTS was used to observe the surface species over K-Bir and Fe-Bir when they were exposed to a flow of 80 ppm HCHO/O_2 for 60 min at room temperature (**Fig. 8**). With the increase of exposure time, peaks located around 1343, 1372, 1564 and 2858 cm^{-1} accumulated on both K-Bir and Fe-Bir, which can be assigned to ν_s(COO), δ(CH), ν_{as}(COO), ν(CH) of formate species.[5,34]. Busca et al.[35] reported the formation of dioxymethylene, formate, and methoxide species after adsorption of formaldehyde on different metal oxides. However, in our experiments, only formate species were observed on as-synthesized birnessite samples, which indicates that dioxymethylene and methoxide are easily oxidized to formate and formate is the main intermediate during formaldehyde oxidation process. Peaks located at 1508 and 1314 cm^{-1} can be assigned to carbonate species adsorbed in the monondentate form.[34] However, carbonate species only appeared over K-Bir, and it was not observed over Fe-Bir, which indicate that formate can be further oxidized into carbonate species on K-Bir and not or very slowly on Fe-Bir. The intensity of formate peak was much higher over Fe-Bir than that over K-Bir, which on one hand is due to higher -OH content of Fe-Bir demonstrated by XPS measurement, and on other hand due to the slower further oxidation of formate. In addition, negative peaks around 3591/3694 cm^{-1} over K-Bir and 3581/3696 cm^{-1} over Fe-Bir, which are assigned to -OH species [5,34], were observed. These results indicate that the amount of surface hydroxyl groups decreased during HCHO oxidation. It has been reported that -OH plays a key role during HCHO oxidation in the formation of formate and its further oxidation to CO_2 and H_2O.[4,5,9]

To further learn the role of surface hydroxyl group and its regeneration during HCHO oxidation, after the exposure of 80 ppm HCHO/O_2 for 60 min, the samples were purged with dry O_2 for 60 min. As can be seen from **Fig. 8**, no obvious changes happened for both K-Bir and Fe-Bir, which indicates that intermediates was not further oxidized under dry O_2 atmosphere. However, when the samples were purged with humid O_2 gas (H_2O/O_2), the absorption spectra of K-Bir changed dramatically. As seen in **Fig. 8a**, peaks of δ(CH) and ν(CH), i.e. located at 1372 and 2858 cm^{-1} disappeared completely. Peaks of ν_s(COO) and ν_{as}(COO), i.e. at 1343 and 1564 cm^{-1} also greatly decreased. In addition, there was a new peak located at 1414 cm^{-1}, which is assigned to HCO_3^-.[36,37] As we know, HCO_3^- is more easily to be desorbed.[38] In addition, peaks of hydroxyl group partly recovered, which is consistent with the report in literature that surface -OH can be supplemented through the reaction between water and surface

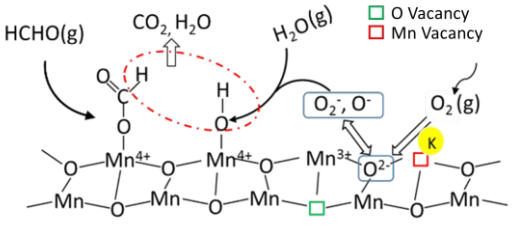

Fig. 10. Reaction pathway of HCHO on the K-Bir catalyst.

O. [9] These phenomena indicate that the accumulated formate species over K-Bir were further oxidized under humid O_2 atmosphere, simultaneously carbonate species were desorbed and transformed to HCO_3^-, and consumed hydroxyl groups were partly regenerated. However, as for Fe-Bir (**Fig. 8b**), though surface hydroxyl groups were significantly recovered after H_2O/O_2 purging, the shape and intensity of the spectra of formate species were almost unchanged. The new peaks at 1662 and ~ 3100 cm^{-1} can be assigned to the vibration absorption of H_2O. These results indicate that, though Fe-Bir owned higher content of -OH, leading to its highest HCHO removal efficiencyvia adsorption and transformation of HCHO into formate, it had low ability to oxidize formate into CO_2, and water vapor could not stimulate further oxidation of formate either. According to the above facts, we conclude that surface -OH over K-Bir and Fe-Bir both exhibit the ability to transform HCHO into formate, while only that over K-Bir has the strong ability to further oxidize formate to CO_2 at room temperature. Thus, besides the content of surface -OH owned by birnessite, there is other more important factor responsible for the complete and sustainable oxidation of HCHO at room temperature.

H_2-TPR and O_2-TPD

To differentiate the activity of surface oxygen in different birnessite samples, their reducibility was evaluated by H_2-TPR. As shown in **Fig. 9a**, H_2-TPR profile can be deconvoluted into four peaks, i.e. α, β, γ and δ. Among them, α peak is assigned to the consumption of surface active oxygen, while β, γ and δ peak correspond to the stepwise reduction of MnO_2 to Mn_2O_3, Mn_2O_3 to Mn_3O_4, and Mn_3O_4 to MnO.[39] The proportion of these three peaks is about 3:1:2. As seen in **Fig. 9a**, the reduction temperature of α peak for K-Bir, Mg-Bir, Ca-Bir and Fe-Bir are 162, 249, 217 and 225 °C, respectively. K-Bir showed the lowest onset reduction temperature among all samples, implying the easiest reducibility of its surface oxygen, i.e. the highest oxidation potential. It is consistent with its highest CO_2 conversion efficiency. Besides, the lattice oxygen in K-O-Mn bond exhibited a downward tendency due to the presence of K^+. Hou et.al [22] also reported that the introduction of K ions into OMS-2 promotes the mobility of lattice oxygen via electronic delocalization effect. It can be concluded that the surface oxygen on K-Bir showed the best hydrogen reduction ability, which may be responsible for HCHO oxidation.

O_2-TPD was also used to investigate the activation of O_2 over birnessite samples with different interlayer cations (**Fig. 9b**). There were several broad O_2 desorption peaks from 40 °C to 500 °C. The first peak was caused by the desorption of surface chemsisobed oxygen (O_2^-, O^- etc.) which was formed through the conversion of surface lattice oxygen around the vacancy, while the rest were attributed to the release of lattice oxygen. The first O_2 desorption occurred at temperatures of 118, 168, 187 and 196 °C for K-Bir, Ca-Bir, Mg-Bir and Fe-Bir, respectively. K-Bir showed the lowest O_2 desorption temperature. These results further confirmed that the presence of K ions enhanced the mobility and activation of the chemisorbed oxygen over the birnessite, which contribute to the activity for HCHO oxidation.

According to the above results, the reaction pathway of HCHO over K-Bir is illustrated in **Fig. 10**. Surface -OH plays a critical role in the HCHO oxidation. First, HCHO is adsorbed and transformed to formate species ($HCOO^-$) on the surface via the participation of surface oxygen and surface hydroxyl (-OH). Then formate species further react with surface -OH on the surface of birnessite to form CO_2 and H_2O ($CHOO^- + OH^- \rightarrow CO_2 + H_2O$), which has been reported in literatures.[5,6,8,9] As for birnessite samples with different interlayer cations, formate species was accumulated with the consumption of surface -OH for long term use. However, surface -OH can be regenerated via the reaction between surface active oxygen (O_2^-, O^- etc.) and water vapor (O_2^-, $O^- + H_2O \rightarrow 2\text{-}OH$). Apart from Mn vacancy, O vacancy is also commonly accompanied with the appearance of Mn^{3+} in birnessite.[28,40] Surface active chemisorbed oxygen (O_2^-, O^- etc.) can be formed by the complex migration between surface O^{2-} and oxygen vacancy with the continuous dissociation of molecular oxygen.[41,42] The reactivity of surface oxygen depends on the surrounding chemical environment. Surface oxygen associated with the Mn and K ions tends to be more reducible at low temperatures, therefore, surface oxygen in K-Bir is more active to react with H_2O to compensate the consumption of -OH species.

Conclusion

In summary, four kinds of birnessite samples with different interlayer cations (K^+, Mg^{2+}, Ca^{2+}, Fe^{3+}) were synthesized by facile redox reaction. The activity of as-synthesized birnessite toward HCHO oxidation at ambient temperature was significantly influenced by the interlayer cations. Fe-Bir showed highest HCHO removal efficiency due to its highest content of -OH while K-Bir showed highest CO_2 conversion efficiency due to its more active surface oxygen. The introduction of potassium ions enhances the activity of surface oxygen, which can react with H_2O to compensate the consumption of -OH, therefore, resulting the continuous and complete oxidation of HCHO. These findings will be helpful to design and prepare high efficient catalyst for HCHO oxidation at room temperature by incorporating different cations into transition metal oxides.

Acknowledgements

This work was funded by the National High Technology Research and Development Program of China (2012AA062701), National Nature Science Foundation of China (21221004, 21411140032) and Tsinghua University Initiative Scientific Research Program (20131089251).

Notes and references

1 T. Salthammer, S. Mentese and R. Marutzky, Chem. Rev., 2010, 110, 2536-2572.

2 T. J. Quiroz, S. Royer, J. P. Bellat, J. M. Giraudon and J. F. Lamonier, Chem. Sus. Chem., 2013, 6, 578-592.
3 M. A. Sidheswaran, H. Destaillats, D. P. Sullivan, J. Larsen and W. J. Fisk, Appl. Catal., B, 2011, 107, 34-41.
4 L. Nie, J. Yu, X. Li, B. Cheng, G. Liu and M. Jaroniec, Environ. Sci. Technol., 2013, 47, 2777-2783.
5 C. Zhang, F. Liu, Y. Zhai, H. Ariga, N. Yi, Y. Liu, K. Asakura, M. Flytzani-Stephanopoulos and H. He, Angew. Chem., Int. Ed., 2012, 51, 9628-9632.
6 H. Huang and D. Y. C. Leung, Acs Catal., 2011, 1, 348-354.
7 C. Zhang, Y. Li, Y. Wang and H. He, Environ. Sci. Technol., 2014, 48, 5816-5822.
8 Q. Xu, W. Lei, X. Li, X. Qi, J. Yu, G. Liu, J. Wang and P. Zhang, Environ. Sci. Technol., 2014, 48, 9702-9708.
9 B. Chen, X. Zhu, M. Crocker, Y. Wang and C. Shi, Appl. Catal., B, 2014, 154, 73-81.
10 Y. Sekine, Atmos. Environ., 2002, 36, 5543-5547.
11 H. Chen, J. He, C. Zhang and H. He, J. Phys. Chem. C, 2007, 111, 18033-18038.
12 H. Tian, J. He, X. Zhang, L. Zhou and D. Wang, Micro. Meso. Mater., 2011, 138, 118-122.
13 R. Averlant, S. Royer, J. M. Giraudon, J. P. Bellat, I. Bezverkhyy, G. Weber and J. F. Lamonier, Chem. Cat. Chem., 2014, 6, 152-161.
14 X. Tang, Y. Li, X. Huang, Y. Xu, H. Zhu, J. Wang and W. Shen, Appl. Catal., B, 2006, 62, 265-273.
15 C. Shi, Y. Wang, A. Zhu, B. Chen and C. Au, Catal. Commun., 2012, 28, 18-22.
16 J. Miyawaki, G. Lee, J. Yeh, N. Shiratori, T. Shimohara, I. Mochida and S. Yoon, Catal. Today, 2012, 185, 278-283.
17 T. Chen, H. Dou, X. Li, X. Tang, J. Li and J. Hao, Micro. Meso. Mater., 2009, 122, 270-274.
18 J. Wang, P. Zhang, J. Li, C Jiang, R. Yunus, J. Kim, Envir. Sci. Technol., 2015, 49, 12372-12379.
19 E. A. Johnson and J. E. Post, Am. Mineral., 2006, 91, 609-618.
20 J. K. Nørskov, T. Bligaard, B. Hvolbæk, F. Abild-Pedersen, I. Chorkendorff and C. H. Christensen, Chem. Soc. Rev., 2008, 37, 2163−2171.
21 B. Bai and J. Li, ACS. Catal., 2014, 4, 2753-2762.
22 J. Hou, L. Liu, Y. Li, M. Mao, H. Lv and X. Zhao, Environ. Sci. Technol., 2013, 47, 13730-13736.
23 F. Xu, Z. Huang, P. Hu, Y. Chen, L. Zheng, J. Gao and X. Tang, Chem. Commun., 2015.
24 M. Wiechen, I. Zaharieva, H. Dau and P. Kurz, Chem. Sci., 2012, 3, 2330-2339.
25 H. Matsui, J. Ju, T. Odaira and N. Toyota, J. Jap. Phys. Soc., 2009, 78.
26 N. N. Greenwood and A. Earnshaw, Chemistry of the Elements, Butterworth-Heinemann, Oxford, 1997.
27 J. E. Post and D. R. Veblen, Amer. Mineral., 1990, 75, 477–489.
28 H. Wang, J. Zhang, Xu. Hang, X. Zhang, J. Xie, B. Pan and Y. Xie, Angew. Chemie., 2015, 127, 1211-1215.
29 K. D. Kwon, K. Refson and G. Sposito, Phys. Rev. Lett., 2008, 100, 146601.
30 K. D. Kwon, K. Refson and G. Sposito, Geochim. Cosmochim. Acta., 2013, 101, 222-232.
31 M. C. Biesinger, B. P. Payne, A. P. Grosvenor, L. W. M. Lau, A. R. Gerson and R. S.C. Smart, Appl. Surf. Sci., 2011, 25, 2717-2730.
32 T. Mathew, K. Suzuki, Y. Ikuta, N. Takahashi and H. Shinjoh, Chem. Commun., 2012, 48, 10987-10989.
33 K. D. Kwon, K. Refson, G. Sposito, Geochim. Cosmochim. Acta., 2009, 73, 4142-4150.
34 J. Quiroz, J. M. Giraudon, A. Gervasini, C. Dujardin, C. Lancelot, M. Trentesaux and J. F. Lamonier, ACS Catal. 2015, 5, 2260-2269.
35 G. Busca, J. Lamotte, J.C. Lavalley, V. Lorenzelli, J. Am. Chem. Soc. 1987, 109, 5197-5202.
36 D. D. Davydov and C. H. Rochester, John Wiley& Sons Press: Chichester, New York, Brisbane, Toronto, Singapore, 1990.
37 L. Liu, H. Zhao, J.M. Andino and Y. Li, ACS. Catal., 2012, 2, 1817-1828.
38 D. Z. Zhao, C. Shi, X. S. Li, A, M. Zhu and B. W. L. Jang, J. Hazard. Mater., 2012, 239, 362-369.
39 P. Hu, Z. Amghouz, Z. Huang, F. Xu, Y. Chen and X. Tang, Environ. Sci. Technol., 2015, 49, 2384−2390.
40 J. Hou, Y. Li, M. Mao, L. Ren, X. Zhao, ACS Appl. Mater. Interfaces, 2014, 6, 14981-14987.
41 H. Over, A.P. Seitsonen, Science, 2002, 297, 2003−2005.
42 B. Bai, J, Li, ACS Catal., 2014, 4, 2753-2762.